LETTERS
PUBLISHED ONLINE: 16 DECEMBER 2012 | DOI: 10.1038/NPHOTON.2012.313
nature photonics

Direct determination of the transition to localization of light in three dimensions

T. Sperling[1], W. Bührer[1], C. M. Aegerter[2]* and G. Maret[1]

Diffusive wave transport in three-dimensional media should show a phase transition, with increasing disorder, to a state without transport. This transition was first discussed by Anderson[1] in the context of the metal–insulator transition, but is generic for all waves, as was realized later[2,3]. However, the quest for the experimental demonstration of 'Anderson' localization in three dimensions has been a challenging task. For electrons[4] and cold atoms[5,6], the challenge lies in the possibility of bound states in a disordered potential. Therefore, electromagnetic and acoustic waves have been the prime candidates for the observation of Anderson localization[7–17]. The main challenge in using light lies in the distinction between the effects of absorption and localization[11,12]. Here, we present measurements of the time dependence of the transverse width of the transmitted-light intensity distribution, which provides a direct measure of the localization length, independent of absorption. This provides direct evidence for a localization transition in three dimensions.

In the diffusive regime ($kl^* \gg 1$) the mean-square width σ^2 of the transmitted pulse, that is, the spread of the photon cloud, is described by a linear increase in time $\sigma^2 = 4Dt$ (ref. 17). Here, D is the diffusion coefficient for light, k is the wave vector and l^* is the transport mean free path. When considering the interference effects of diffusive light, Anderson and colleagues[19] predicted a transition to localization in three-dimensional systems at a high enough turbidity $(kl^*)^{-1}$. The criterion for where this transition should occur is known as the Ioffe–Regel criterion, namely $kl^* \lesssim 1$ (ref. 20). At such high turbidities light will be localized to regions of a certain length scale, namely the localization length ξ, which diverges at the transition to localization. This implies that σ^2 initially increases linearly with time, but saturates at a later time t_{loc} (localization time) towards a constant value given by $\sigma^2 = \xi^2$.

In this Letter we present measurements of light transport in three-dimensional, open, highly scattering TiO_2 powders. Given the high turbidity of the samples studied and the large slab thickness (L varying from 0.6 mm to 1.5 mm), the transmitted light typically undergoes a few million scattering events in any of the three spatial directions before leaving the sample. Our samples therefore also present a true bulk three-dimensional medium for light transport.

The great advantage of determining the time dependence of the width of the transmission profile is that because the width is obtained at a specified time, absorption effects are equally present on all paths. This means that the width of the profile at a given time is independent of absorption. This can be seen from the general definition of the width in terms of the spatial dependence of the photon density $T(\rho, t)$, where ρ is a vector in the two-dimensional transmission plane with the origin at the centre of the beam: $\sigma^2(t) = \int \rho^2 T(\rho, t)\mathrm{d}^2\rho / \int T(\rho, t)\mathrm{d}^2\rho$. In this definition, an exponential decrease due to absorption enters $T(\rho, t)$ both in the nominator and in the denominator and thus cancels out. In the diffusive regime, the profile will be given by a Gaussian—$T(\rho) \propto \exp(-\rho^2/8Dt)$—that is, with a width $\sigma^2 = 4Dt$. We therefore fit a two-dimensional Gaussian to the intensity profile at a given time (see Fig. 1, which shows the gated intensity profile at three different time points, demonstrating the increase in width with time). This fit yields the width of the Gaussian in both the x- and y-directions. In localizing samples, the intensity distribution is expected to be exponential with a characteristic length scale ξ. This can be seen in our samples. However, at small distances ρ, the profile can be well approximated by a Gaussian (Supplementary Section IV, Fig. S4). Accordingly, we fit a Gaussian to all our samples, giving fits that are qualitatively similar to an exponential function in the localized case (Supplementary Section IV, Fig. S5).

The fitted widths were then plotted as a function of time to yield the results shown in Fig. 2a–c. In the case of a diffusive sample (Aldrich anatase) with $kl^*_{AA} = 6.4$, the square of the width increases linearly over the whole timespan (Fig. 2a), as expected. The small deviation from linearity around the diffusion time $\tau_{\max}$ is a result of the gating of the high rate intensifier (HRI) (Supplementary Section II, Fig. S3). The slope of the increase is in good agreement with the diffusion coefficient determined from time-dependent transmission experiments[14] (Supplementary Table S1). Note also that the time-dependent width can exceed the thickness of the sample, which is a result of the fact that we are studying the transmission profile at specific times.

The width σ^2 of the transmitted pulse gives a direct measure of the localization length ξ in the localizing regime. This is because the two-dimensional transmission profile of the photon cloud is confined to within a localization length. When considering an effective diffusion coefficient corresponding to the slope of the temporal increase in width, one thus obtains an effective decrease of the diffusion coefficient with time as $D(t) \propto 1/t$ after a timescale corresponding to the localization length[21]. In this picture, for large L, one expects a time dependence of σ^2, which is linear up to the localization length and then remains constant as time goes on. Numerical calculations of self-consistent theory[22,23] give a different increase at short times as $\sigma^2 \propto t^{1/2}$ and a plateau value of $\sigma^2 = 2L\xi$ for $L \gg \xi$. These predictions can be directly tested from data of samples with high turbidity, which show non-classical diffusion in time-dependent transmission measurements (Fig. 2b,c). Taking a closer look at the short time behaviour one can see that σ^2 increases linearly in time, contrary to the self-consistent theory calculation. This is similar to the behaviour found in acoustic waves[17]. However, in contrast to the diffusive sample, a plateau of the width can be clearly seen. This is in good accord with the theoretical prediction[23] and a direct sign of Anderson localization. This plateau can also be seen directly from the transmission profiles shown in Fig. 1, where the normalized intensity profile is shown for three

[1]Fachbereich Physik, University of Konstanz, Universitätsstrasse 10, 78457 Konstanz, Germany, [2]Physik-Institut, University of Zürich, Winterthurerstrasse 190, 8057 Zürich, Switzerland. *e-mail: aegerter@physik.uzh.ch

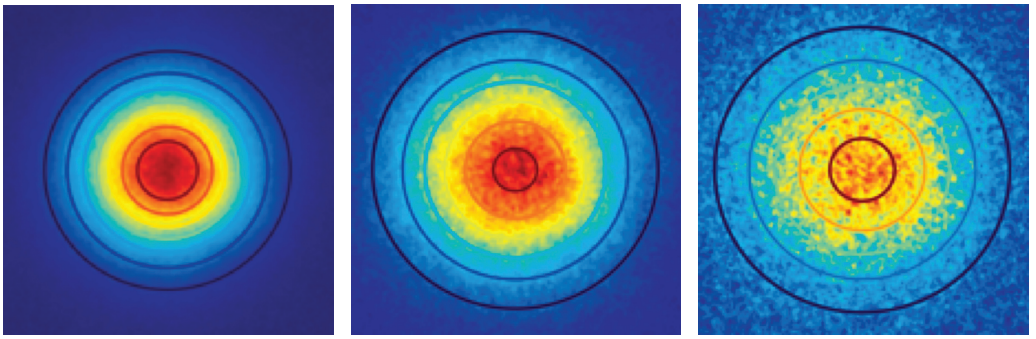

Figure 1 | A section of the raw data (fit displayed via contours) for a R104 sample, featuring a plateau. From left to right the timestamps are 4 ns, 6 ns and 8 ns after the initial laser pulse. From 4 ns to 6 ns one can see a broadening in the profile width, whereas from 6 ns to 8 ns no further increase can be seen. This constant profile width is the signature of Anderson localization.

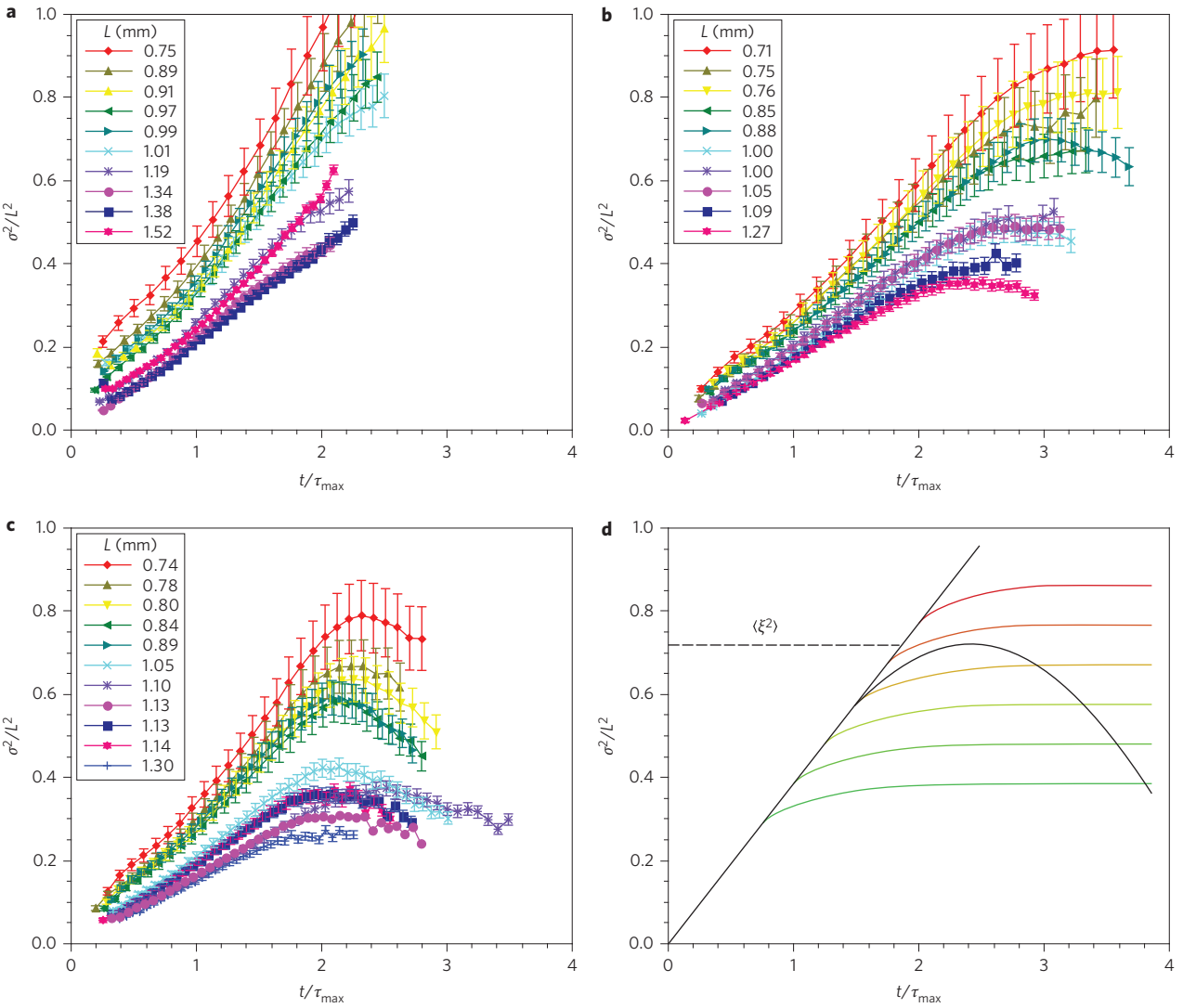

Figure 2 | Time dependence of the mean-square width scaled with sample size σ^2/L^2 for different samples. The time axis is scaled with diffusion time τ_{max} (Supplementary Section III). **a**, Time dependence for Aldrich anatase, which behaves diffusively. **b**,**c**, Time dependence for R104 (**b**) and R700 (**c**) samples, showing localizing effects. **d**, Schematic of expected time dependence of the width in the presence of statistically distributed localization lengths as discussed in the main text. The decreasing population at long times of the modes for larger localization lengths leads to an overall decrease in the width, in particular for sample thicknesses close to the average localization length, because big loops leak out of the sample more than small loops. Different coloured lines represent microscopic localization lengths increasing from small (green) to large (red). All error bars correspond to standard errors.

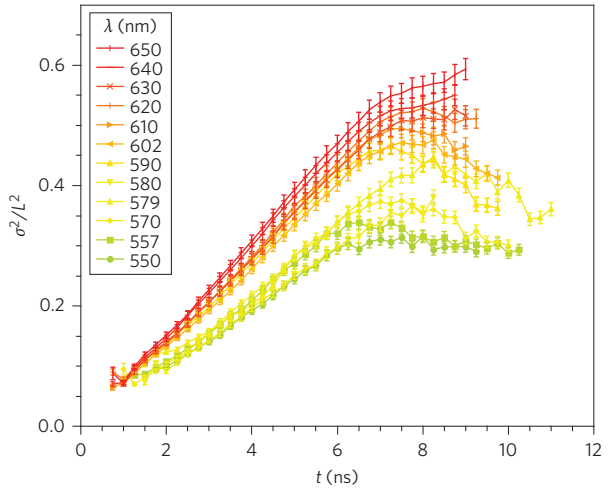

Figure 3 | Spectral measurement of σ^2 for a R700 sample, ranging from 550 nm to 650 nm, corresponding to kl^* values between 2.1 and 3.6. With decreasing wavelength λ the turbidity kl^* increases, and localizing effects become stronger. This can be seen from the lower mean-square widths σ^2_∞ of the plateaux. For wavelengths above 640 nm one can observe a transition from localization to sub-diffusive behaviour. All error bars correspond to standard errors.

different time points. At long times, the width no longer increases, indicating a localization of light.

Figure 2 also presents results for samples of different thickness. These samples were made from the same particles but could vary slightly in terms of filling fraction. However, as checked by coherent backscattering, samples composed of the same particles had very comparable values of turbidity (Supplementary Section I, Fig. S1). If the thickness L of the sample becomes comparable to the localization length, a decrease in the width of the photon distribution with time can be observed. This surprising fact can be understood in a statistical picture of localization, where a range of localization lengths exists in the sample, corresponding to different sizes of closed loops of photon transport. In finite slabs, larger localized loops are more likely to be cut off by the surfaces than small loops, leading to a lower population of such localized states at longer times. Thus, on average, the observed width will correspond to increasingly shorter localization lengths and a decrease of σ^2 with time may therefore occur. This is schematically illustrated in Fig. 2d. Note that such a peak in the width of the intensity distribution has also been seen in calculations of self-consistent theory, albeit in thicker samples[23], such that no direct comparison with our data is possible. When the thickness decreases even more, so that it is shorter than the localization length, the plateau in the width is lost altogether and σ^2 increases over the whole time window. In fact, the behaviour rather corresponds to that predicted for the mobility edge[21], where a sublinear increase of $\sigma^2 \propto t^{2/3}$ is predicted. At the transition, one observes a kink in σ^2 and the ratio of the initial slope to that at the kink corresponds to the sub-diffusive exponent a. In fact, this thickness dependence can be used in an alternative determination of the localization length.

Evaluation of the plateaux of the localizing samples for different thicknesses yields a localization length independent of L. Where the time dependence has a maximum rather than a plateau, the maximum value is used. We identified $\sigma^2_\infty = \xi^2$ and obtained $\xi_{R104} = 717(6)$ μm for R104, $\xi_{R902} = 717(9)$ μm for R902 and $\xi_{R700} = 670(9)$ μm for R700. These are mean values for all thicknesses investigated.

As expected, sample R700 has the smallest localization length ξ (as has already been concluded from time-of-flight experiments[14]), which corresponds to the lowest value of $kl^*_{R700} = 2.7$. In terms of localization, R104 and R902 are very comparable, which again is in good accord with the fact that their turbidities are very similar—$kl^*_{R104} = 3.7$ and $kl^*_{R902} = 3.4$, respectively—even though their other sample properties are rather different. As stated above, this determination of ξ is in good agreement with that from the thickness dependence of the occurrence of a plateau. As seen in Fig. 2, R104 (with a thickness of $L = 0.71$ mm) behaves sub-diffusively, but the sample with $L = 0.75$ mm shows a plateau, indicating a localization length of $\xi = 0.73(2)$ mm. The same transitional behaviour can also be seen for R902 in the range $0.7\ \text{mm} < L < 0.8\ \text{mm}$.

So far, we have shown that for different samples with a range of kl^* close to unity a qualitative change occurs in the transport properties, which is consistent with the transition to Anderson localization. To show that these are not intrinsic properties of the sample, we studied one sample at different incoming wavelengths. The turbidity depends quite strongly on the wavelength λ of light, which we tuned from 550 nm to 650 nm. For these wavelengths, we determined that the turbidity changes from $kl^*_{550\text{nm}} \approx 2.1$ to $kl^*_{650\text{nm}} \approx 3.45$, thus spanning a range similar to that spanned by the different samples considered above. At the highest and lowest wavelengths, the values of kl^* were interpolated from the experimentally accessible values, which is a good approximation, because for the region under investigation, kl^* is found to scale linearly with λ (Supplementary Section I, Fig. S2). The result of such a spectral measurement of a R700 sample ($L = 0.98$ mm and $m = 377$ mg) is shown in Fig. 3. For wavelengths 640 nm and 650 nm, corresponding to the largest values of kl^*, σ^2 does not saturate, whereas it does for smaller kl^*, which pinpoints the mobility edge. This allows a direct characterization of the localization transition with a continuous change of the control parameter kl^*.

We also determined the same spectral information for a R104 sample, which is closer to the mobility edge at a wavelength of 590 nm, and for a rutile sample from Aldrich, which shows classical diffusion at 590 nm. For all these samples we determined the value of kl^* (ref. 24). With the value of ξ and the scattering strength kl^* we are able to determine the approach to the mobility edge at kl^*_{crit}, as shown in Fig. 4. At the mobility edge we can determine the qualitative change in behaviour from the ratio of the slopes of σ^2 as a function of time in the localized or sublinear regime and the initial diffusive regime (Supplementary Section VII). This gives a direct

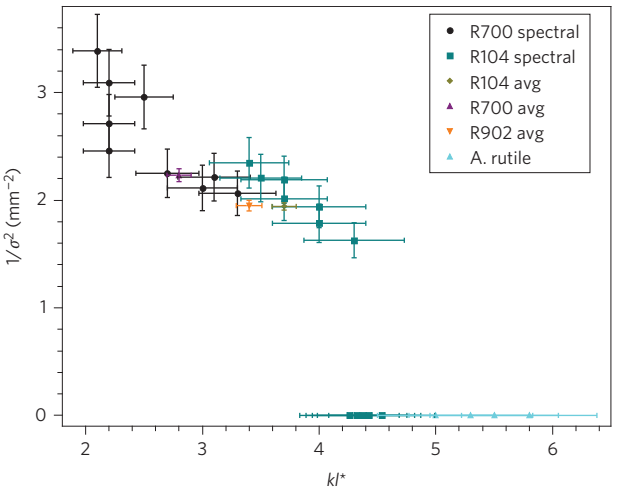

Figure 4 | Inverse of the mean-square width σ^2_∞ of the plateau versus kl^* for different samples. As can be seen, the width (corresponding to the localization length) diverges at $l^* \approx 4.5$, indicating the transition from a localized to a non-localized state. The increase of the localization length approaching the critical turbidity can also be used to estimate the critical exponent. All error bars correspond to systematic errors.

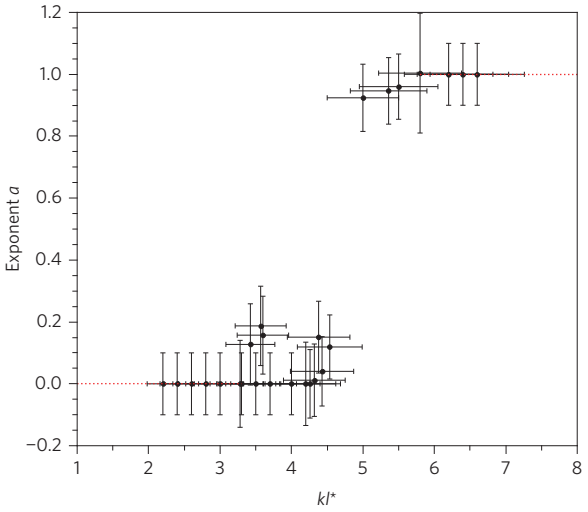

Figure 5 | Value of exponent *a*, describing the temporal increase of the mean-square width (see main text). In the diffusive regime, the exponent should be unity, whereas in the fully localized regime a value of zero is expected. At the mobility edge the sub-diffusive increase corresponds to intermediate values. This allows determination of the critical turbidity. All error bars correspond to standard errors.

estimate of exponent a, with which the width increases with time, $\sigma^2 \propto t^a$ (Fig. 5). There is a clear transition in the behaviour as $kl^\star$ changes, showing a critical value of $kl^\star_{\rm crit} = 4.5(4)$ above which $a = 1$ and below which $a = 0$. This is in good agreement with the results of time-of-flight measurements on similar samples, which yielded $kl^\star_{\rm crit,ToF} = 4.2(2)$ (ref. 14). Note that with a sample effective refractive index of $n_{\rm eff} \approx 1.75$, a critical value of $kl^\star_{\rm crit} = 4.2$ corresponds to an onset of localization at the point $l^\star/\lambda_{\rm eff} \approx 1$, which is a reasonable expectation for the onset of localization.

The dependence of inverse width on turbidity, as shown in Fig. 4, also indicates the critical behaviour around the transition. Below the critical turbidity, σ^2 increases at all times and the corresponding inverse localization length is zero. At the mobility edge, the localization length is limited by the sample thickness, which in the case shown in Fig. 4 was ∼1 mm, and a more detailed determination of the intrinsic localization length is not possible. For highly turbid samples, well below the transition, the inverse localization length seems to increase linearly with decreasing $kl^\star$, indicating an exponent of unity. However, there is insufficient dynamic range close to the transition for a full determination of a critical exponent.

In conclusion, we have shown direct evidence for localization of light in three dimensions and the corresponding transition at the mobility edge. This has been achieved using the time dependence of the mean-square width σ^2 of the transmission profile, which is an excellent measure for the onset of localization of light. In contrast to other measures, it is completely independent of absorption and allows a direct determination of the localization length for samples close to the mobility edge. We find that, for highly turbid samples, σ^2 shows a plateau, which changes to a sublinear increase for critical turbidities and becomes linear for purely diffusive samples. This allows a detailed characterization of the behaviour of transport close to the transition, which is not possible with other techniques. By evaluating the plateau σ^2_∞ of localizing samples one can directly access the localization length ξ. For sample thicknesses close to the localization length, we moreover observe a decrease in the width of the photon cloud, which we associate with a statistical distribution of microscopic localization lengths. These data may stimulate further theoretical work and comparison between such quantitative theories as self-consistent theory[23] or direct numerical simulation[25], and the data may yield valuable information about the statistical distribution of localization lengths close to the transition.

We have also shown that the transition to localization can be observed in one and the same sample using spectral measurements, thus continuously varying the control parameter of turbidity through the transition. For highly turbid samples, the width of the transmission profile saturates at a value that increases with decreasing turbidity until the localization length is comparable to the sample thickness. At this point the width increases at all times, albeit with a sublinear increase at long times. This behaviour is expected from the diffusion coefficient at the mobility edge[21]. Such measurements close to the transition between Anderson localization and diffusion allow a determination of the critical turbidity $kl^\star_{\rm crit} = 4.5(4)$, which is in good agreement with an indirect determination using time-of-flight measurements. In addition, our determination of the localization length during the approach to the localization transition allows an estimate of the critical exponent of the transition. Well away from the critical regime, we find a value close to unity, which is not incompatible with theoretical determinations[3,19,26]. A complete description of the transition in open media taking finite size effects into account will be a great challenge for future theoretical descriptions of Anderson localization.

Methods

The samples were slabs composed of nanoparticles with diameters ranging from 170 nm to 540 nm and polydispersities ranging between 25% and 45%. Powders were provided by DuPont and Sigma Aldrich. These samples are slightly compressed and have been used previously[14] to demonstrate non-classical transport behaviour in time-dependent transmission. TiO_2 has a relatively high refractive index in the visible of $n = 2.7$ in the rutile phase and $n = 2.5$ in the anatase phase.

The extremely high turbidity of the samples necessitates the use of a high-power laser system in order to be able to measure the transmitted light. We used a frequency-doubled Nd:YAG laser (Verdi V18) operating at an output power of 18 W to pump a Ti:sapphire laser (HP Mira). The HP Mira was operated mode-locked with a repetition rate of 75 MHz at a maximum power of ∼4 W. To convert the laser light from ∼790 nm to orange laser light (590 nm), a frequency-doubled optical parametric oscillator (OPO) was used. The laser wavelength emitted by the OPO could be tuned from ∼550 nm to 650 nm.

To approximate a point-like source the laser beam was focused onto the flat front surface of the sample with a waist of 100 μm. The transmitted light was imaged from the flat backside by a magnifying lens ($f = 25$ mm, mounted in reverse position) onto an HRI (LaVision PicoStar). The HRI could be gated on a timescale of ∼1 ns and the gate could be shifted in time steps of 0.25 ns. The HRI was made of gallium arsenide phosphide, which has a high quantum efficiency with a maximum of 40.6% at ∼590 nm. A fluorescent screen imaged the signal onto a 16-bit charge-coupled device camera with a resolution of 512 × 512 pixel. With this system we were able to record the transmitted profile with a time resolution below a nanosecond.

To measure the turbidity of a sample we used a backscattering set-up as described elsewhere[13,24]. With this set-up covering the full angular range, it was possible to determine $kl^\star$ from the inverse width of the backscattering cone. As this system used different laser sources, the spectral range of the set-up was more limited in wavelength (568 nm to 619 nm and 660 nm).

Received 5 July 2012; accepted 8 November 2012;
published online 16 December 2012

References

1. Anderson, P. W. Absence of diffusion in certain random lattices. *Phys. Rev.* **109,** 1492–1505 (1958).
2. Anderson, P. W. The question of classical localization: a theory of white paint? *Phil. Mag. Lett.* **52,** 505–509 (1985).
3. John, S. Electromagnetic absorption in a disordered medium near a photon mobility edge. *Phys. Rev. Lett.* **53,** 2169–2172 (1984).
4. Altshuler, B. L. *et al. Mesoscopic Phenomena in Solids* (North-Holland, 1991).
5. Kondov, S. S. *et al.* Three-dimensional Anderson localization of ultracold matter. *Science* **334,** 66–68 (2011).
6. Jendrzejewski, F. *et al.* Three-dimensional localization of ultracold atoms in an optical disordered potential. *Nature Phys.* **8,** 398–403 (2012).
7. Kuga, Y. & Ishimaru, A. Retroreflectance from a dense distribution of spherical particles. *J. Opt. Soc. Am. A* **1,** 831–835 (1984).
8. van Albada, M. P. & Lagendijk, A. Observation of weak localization of light in a random medium. *Phys. Rev. Lett.* **55,** 2692–2695 (1985).

9. Wolf, P. E. & Maret, G. Weak localization and coherent backscattering of photons in disordered media. *Phys. Rev. Lett.* **55,** 2696–2699 (1985).
10. Drake, J. M. & Genack, A. Z. Observation of nonclassical optical diffusion. *Phys. Rev. Lett.* **63,** 259–262 (1989).
11. Wiersma, D. S., Bartolini, P., Lagendijk, A. & Righini, R. Localization of light in a disordered medium. *Nature* **390,** 671–673 (1997).
12. Scheffold, F., Lenke, R., Tweer, R. & Maret, G. Localization or classical diffusion of light? *Nature* **398,** 206–270 (1999).
13. Fiebig, S. *et al.* Conservation of energy in coherent backscattering at large angles. *Europhys. Lett.* **81,** 64004 (2008).
14. Störzer, M., Gross, P., Aegerter, C. M. & Maret, G. Observation of the critical regime in the approach to Anderson localization of light. *Phys. Rev. Lett.* **96,** 063904 (2006).
15. Aegerter, C. M., Störzer, M. & Maret, G. Experimental determination of critical exponents in Anderson localization of light. *Europhys. Lett.* **75,** 562–568 (2006).
16. Bayer, G. & Niederdränk, T. Weak localization of acoustic waves in strongly scattering media. *Phys. Rev. Lett.* **70,** 3884–3887 (1993).
17. Hu, H., Strybulevych, A., Page, J. H., Skipetrov, S. E. & van Tiggelen, B. A. Localization of ultrasound in a three-dimensional elastic network. *Nature Phys.* **4,** 945–948 (2008).
18. Lenke, R. & Maret, G. *Multiple Scattering of Light: Coherent Backscattering and Transmission* (Gordon & Breach, 2000).
19. Abrahams, E., Anderson, P. W., Licciardello, D. C. & Ramakrishnan, T. V. Scaling theory of localization: absence of quantum diffusion in two dimensions. *Phys. Rev. Lett.* **42,** 673–676 (1979).
20. Ioffe, A. F. & Regel, A. R. Non-crystalline, amorphous and liquid electronic semiconductors. *Prog. Semicond.* **4,** 237–291 (1960).
21. Berkovits, R. & Kaveh, M. Propagation of waves through a slab near the Anderson transition: a local scaling approach. *J. Phys. C* **2,** 307–321 (1990).
22. Skipetrov, S. E. & van Tiggelen, B. A. Dynamics of Anderson localization in open 3D media. *Phys. Rev. Lett.* **96,** 043902 (2006).
23. Cherroret, N., Skipetrov, S. E. & van Tiggelen, B. A. Transverse confinement of waves in random media. *Phys. Rev. E* **82,** 056603 (2010).
24. Gross, P. *et al.* A precise method to determine the angular distribution of backscattered light to high angles. *Rev. Sci. Instrum.* **78,** 033105 (2007).
25. Gentilini, S., Fratalocchi, A. & Conti, C. Signatures of Anderson localization excited by an optical frequency comb. *Phys. Rev. B.* **81,** 014209 (2010).
26. MacKinnon, A. & Kramer, B. One-parameter scaling of localization length and conductance in disordered systems. *Phys. Rev. Lett.* **47,** 1546–1549 (1981).

Acknowledgements

This work was funded by Deutsche Forschungsgemeinschaft, Swiss National Science Foundation and the Land Baden-Württemberg via the Center for Applied Photonics. The authors thank N. Cherroret for support and fruitful discussions.

Author contributions

T.S., W.B., C.M.A. and G.M. conceived and designed the experiments. T.S. and W.B. carried out the experiments. T.S., W.B., C.M.A. and G.M. analysed and interpreted the data. T.S., W.B., C.M.A. and G.M. wrote the manuscript.

Additional information

Supplementary information is available in the online version of the paper. Reprints and permission information is available online at http://www.nature.com/reprints. Correspondence and requests for materials should be addressed to C.M.A.

Competing financial interests

The authors declare no competing financial interests.